Univerzita Komenského v Bratislave

Fakulta matematiky, fyziky a informatiky

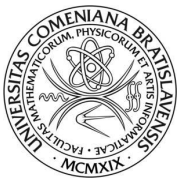

Mgr. Tomáš Dado

Autoreferát dizertačnej práce

Direct measurement of the top-quark decay width with the ATLAS detector

na získanie akademického titulu *philosophiae doctor*

v odbore doktorandského štúdia: 4.1.5. Jadrová a subjadrová fyzika

BRATISLAVA, 2019

Dizertačná práca bola vypracovaná v dennej forme doktorandského štúdia na
Katedre jadrovej a subjadrovej fyziky
Fakulty matematiky, fyziky a informatiky
Univerzity Komenského v Bratislave.

Predkladateľ: Mgr. Tomáš Dado
Katedra jadrovej fyziky a biofyziky
Fakulta, matematiky, fyziky a informatiky
Univerzity Komenského
Mlynská dolina
842 48 Bratislava

Školiteľ: prof. RNDr. Stanislav Tokár, CSc.
Katedra jadrovej fyziky a biofyziky
FMFI UK Bratislava

Oponenti:

Obhajoba dizertačnej práce sa koná dňa ..... o ..... h pred komisiou pre obhajobu dizertačnej práce v odbore doktorandského štúdia vymenovanou predsedom odborovej komisie dňa ..... .

4.1.5. Jadrová a subjadrová fyzika

Predseda odborovej komisie:

prof. RNDr. Jozef Masarik, DrSc.
Katedra jadrovej fyziky a biofyziky
Fakulta, matematiky, fyziky a informatiky
Univerzity Komenského
Mlynská dolina
842 48 Bratislava

Abstract

Direct measurement of the top-quark decay width with the ATLAS detector

The top quark is the heaviest known elementary particle. Due to its large mass, the top quark decays before it forms bound states. This makes the top quark a unique particle in the Standard Model. Precise measurements of its properties could be used as tests of the consistency of the Standard Model and potential deviations could point to physics Beyond the Standard Model. This thesis deals with the direct measurement of the top-quark decay width using data collected in proton-proton collisions at centre-of-mass energies of 8 and 13 TeV with the ATLAS detector at the Large Hadron Collider. The thesis focuses on the more recent measurement at 13 TeV while the most important highlights of the 8 TeV measurement are summarised. The decay width of the top quark is extracted from the data using likelihood fit of distributions of variables sensitive to the top-quark decay width in $t\bar{t}$ pair production. The measurement is performed in a direct way, thus it is less model-dependent compared to indirect methods.

Key words: ATLAS experiment, top quark, decay width

Abstrakt

Priame meranie rozpadovej šírky top kvarku na experimente ATLAS

Top kvark je najťažšia známa elementárna častica. Vďaka svojej veľkej hmotnosti sa top kvark rozpadá skôr ako vytvorí viazané stavy. Táto vlastnosť robí top kvark unikátnou časticou v Štandardnom Modeli. Presné merania vlastností top kvarku sa môžu využiť ako testy konzistentnosti Štandardného Modelu a prípadné odchýlky možu poukázať na fyziku za Štandardným Modelom. Táto práca sa venuje priamemu meraniu rozpadovej šírky top kvarku na dátach z protón-protónových zrážok pri ťažiskovej energii 8 a 13 TeV získaných detektorom ATLAS na urýchľovači LHC. Práca sa zameriava na analýzu dát pri energii 13 TeV, pričom sú však spomenuté aj najdôležitejšie výsledky z analýzy vykonanej na dátovej vzorke s ťažiskovou energiou 8 TeV. Rozpadová šírka top kvarku je získaná z dát pomocou fitu rozdelení premenných citlivých na rozpadovú šírku top kvarku v produkcií top kvarkových párov. Ide o tzv. priame meranie top kvarkovej šírky, ktoré je menej modelovo závislé ako nepriame merania.

Kľúčové slová: ATLAS experiment, top kvark, rozpadová šírka

1 The top quark and its decay width

With its mass around 173 GeV [1], the top quark is the heaviest known elementary particle of the SM. Because of this large mass the top-Higgs Yukawa coupling is $y_t \sim 1$ which suggests that the top quark plays an important role in the spontaneous symmetry breakdown mechanism. The precise measurement of the top-quark decay width, Γ_t, or its mean lifetime, τ_t – these two quantities are trivially connected via $\tau_t = 1/\Gamma_t$ – is the topic of this thesis but the order of magnitude expectation for the top-quark mean lifetime yields $\tau_t \approx 10^{-25}$ s [1]. This is important since the average time needed for the top quark to hadronise is of the order of 10^{-24} s [2] and thus the top quark decays before it forms bound states. This makes the top quark unique among other quarks, as it provides an opportunity to study a pseudo-bare quark.

Top quarks are predominantly produced in pairs via the strong interaction, however, also electroweak processes contribute to the pair production cross section, but the contribution is below the theoretical uncertainty on the pair cross-section originating from the PDF uncertainty [3] and can thus be neglected. Theoretical calculations of $t\bar{t}$ cross-section [4–8] at next-to-next-to-leading order (NNLO) with next-to-next-to-leading resumation of logarithmic soft gluon terms (NNLL) are computed using `top++2.0` program [9]. The latest calculations take advantage of MSTW2008 68 % CL NNLO PDF set [10] with the mass of the top quark set to $m_t = 172.5$ GeV, predictions for Tevatron at $\sqrt{s} = 1.98$ TeV use $m_t = 173.3$ GeV. The uncertainties on the predictions originate from variations of renormalisation and factorisation scales as well as an uncertainty from PDF.

The top quark decays via the weak interaction to a W boson and a down-type quark, $t \to W^+q$ ($\bar{t} \to W^-\bar{q}$). The global measured W boson decay width reads $\Gamma_W = 2.085 \pm 0.042$ GeV [1] which makes also the W boson possible to measure only via its decay products. The W boson decays in 67.4 % into hadrons [1], and in the remaining cases it decays into a charged lepton and a corresponding neutrino. The decay channels of the $t\bar{t}$ pair can thus be characterised by the subsequent decays of the W boson from individual top (anti-)quark decays into three channels: dilepton, lepton+jets and all-hadronic.

The total top-quark decay width is usually calculated only from $t \to Wb$ process which is a very good approximation in the SM. At LO and assuming the mass of the b quark to be $m_b = 0$, the decay width of $t \to Wb$, $\Gamma(t \to Wb)$, yields

$$\Gamma(t \to Wb) = \frac{G_\mathrm{F}}{8\pi\sqrt{2}} m_t^3 \left(1 - \frac{m_W^2}{m_t^2}\right)^2 \left(1 + 2\frac{m_W^2}{m_t^2}\right), \tag{1.1}$$

where G_F is the Fermi constant, $G_\mathrm{F} = 1.1663787(6)10^{-5}$ GeV^{-2} [1] and $m_t(m_W)$ is the top-quark (W boson) mass. Equation 1.1 shows that in the SM the decay width

of the top quark depends on the top-quark mass in third power. Plugging back V_{tb}, Equation 1.1 can be rewritten [11]

$$\Gamma(t \to Wb) = \frac{G_{\mathrm{F}}}{8\pi\sqrt{2}} m_t^3 |V_{tb}|^2 \left(1 - 3\left(\frac{m_W}{m_t}\right)^4 + 2\left(\frac{m_W}{m_t}\right)^6\right). \tag{1.2}$$

The most precise theoretical calculation of the top-quark decay width includes NLO electroweak corrections and effects of finite b-quark mass and finite W boson mass on top of the NLO and NNLO QCD corrections [12].

The most precise theoretical calculation of the top-quark decay width includes NLO electroweak corrections and effects of finite b-quark mass and finite W boson mass on top of the NLO and NNLO QCD corrections [12]. The calculation is presented in the form of corrections to the LO decay width value, $\Gamma_t^{(0)}$, from Equation 1.2

$$\Gamma_t = \Gamma_t^{(0)} \left(1 + \delta_{\mathrm{QCD}}^{(1)} + \delta_{\mathrm{QCD}}^{(2)} + \delta_{\mathrm{EW}} + \delta_f^b + \delta_f^W\right), \tag{1.3}$$

where $\delta_{\mathrm{QCD}}^{(1)}(\delta_{\mathrm{QCD}}^{(2)})$ represents NLO(NNLO) QCD corrections. Contributions from finite b-quark mass are included in δ_f^b and contributions from finite W boson width enter δ_f^W. The effect from individual correction on the top-quark decay width for different input top-quark masses is summarised in Table 1.1.

m_t [GeV]	$\Gamma_t^{(0)}$ [GeV]	$\delta_{\mathrm{QCD}}^{(1)}$ [%]	$\delta_{\mathrm{QCD}}^{(2)}$ [%]	δ_{EW} [%]	δ_f^b [%]	δ_f^W [%]	Γ_t [GeV]
172.5	1.4806	-8.58	-2.09	1.68	-0.26	-1.49	1.3216
173.5	1.5109	-8.58	-2.09	1.69	-0.26	-1.49	1.3488
174.5	1.5415	-8.58	-2.09	1.69	-0.25	-1.48	1.3764

Table 1.1: The SM prediction for the top-quark decay width, Γ_t, for various top-quark masses, m_t. The corrections [12] to LO prediction, $\Gamma_t^{(0)}$, include NLO(NNLO) QCD corrections, $\delta_{\mathrm{QCD}}^{(1)}(\delta_{\mathrm{QCD}}^{(2)})$, NLO electroweak corrections, δ_{EW}, finite mass of the b-quark, δ_f^b and, finally finite width of the W boson, δ_f^W. All corrections are given in percentages.

2 Event Selection

The measurement of the top-quark decay width uses data recorded by the ATLAS detector [13] at a centre-of-mass energy of 13 TeV in proton-proton collisions in years 2015, 2016, 2017 and 2018. The dataset is split into four separate subsets, each corresponding to a different year of data taking. The total luminosity reads $\int L\,dt = 140$ fb^{-1}.

Events passing either of the two considered channels, lepton+jets or dilepton channel, need to pass the following basic selection criteria. Firstly, events need to fire one of the single-lepton triggers for electrons or muons. For 2015 data taking the electron trigger chains are: *HLT_e24_lhmedium_L1EM20VH*, *HLT_e60_lhmedium* and *HLT_e120_lhloose*. Their thresholds correspond to 24 GeV, 60 GeV and 120 GeV, respectively. Muon trigger chains are: *HLT_mu20_iloose_L1MU15* and *HLT_mu50* with 20 GeV and 50 GeV thresholds. Due to increased instantaneous luminosity and pile-up, trigger chains for 2016, 2017 and 2018 data taking have been updated with increased thresholds. The electron trigger chains for 2016, 2017 and 2018 are *HLT_e26_lhtight_nod0_ivarloose*, *HLT_e60_lhmedium_nod0* and *HLT_e140_lhloose_nod0*. The muon trigger chains for 2016, 2017 and 2018 are *HLT_mu26_ivarmedium* and *HLT_mu50*. The increased thresholds of trigger chains require that electrons and muons in 2016, 2017 and 2018 data taking periods are required to have $p_{\mathrm{T}} > 27$ GeV. Furthermore, in the offline selection, the selected lepton (in case of dilepton events one of the selected leptons) needs to match the lepton that fired the trigger for the event to be selected. Additionally, events are required to have at least one primary vertex reconstructed with at least two tracks with $p_{\mathrm{T}} > 400$ MeV matched to this vertex. Events containing fake jets from non-collision background or cosmic events or events containing fake signal in the calorimeter are removed. An overlap procedure is applied to remove multiple reconstructed objects from the same underlying signal and if at least one of the jets fails this cleaning criteria the whole event is rejected.

2.1 Lepton+jets selection

Following the signature of the $t\bar{t}$ signal in the lepton+jets decay channel, the events are expected to have four jets out of which two originate from b-quark, one electron or muon, and one neutrino. Consequently, the selected events are required to have exactly one reconstructed electron or muon with $p_{\mathrm{T}} > 25$ GeV for 2015 data taking and $p_{\mathrm{T}} > 27$ GeV for 2016, 2017 and 2018 data taking. Furthermore, events are required to have at least four reconstructed jets with $p_{\mathrm{T}} > 25$ GeV, with at least two of the reconstructed jets being b-tagged with 60 % efficiency working point of the MV2c10 tagger [14]. The high-purity and low-efficiency b-tagging working point has been chosen to significantly suppress non-$t\bar{t}$ background, especially the W+jets

background. Additionally, requirements on $E_{\mathrm{T}}^{\mathrm{miss}}$ and m_{T}^{W} are imposed. Events are required to have $E_{\mathrm{T}}^{\mathrm{miss}} > 30$ GeV and $m_{\mathrm{T}}^{W} > 30$ GeV for the electron+jets channel and $E_{\mathrm{T}}^{\mathrm{miss}} + m_{\mathrm{T}}^{W} > 60$ GeV for the muon+jets channel. These cuts are chosen to suppress the multijet background, including non-prompt leptons and fake leptons (misidentified leptons).

Moreover, a selection on the reconstruction Boosted Decision Tree (BDT) output, that will be discussed in Chapter 3, is applied requiring the events to have a BDT score > 0.7. This requirement further reduces non-$t\bar{t}$ backgrounds and improves the total precision of the measurement. After the event selection, the events are split into two orthogonal regions according to the charged lepton flavour–into electron+jets and muon+jets events.

2.2 Dilepton selection

Events in the dilepton channel are required to have exactly two leptons (electrons or muons) of opposite electric charge with $p_{\mathrm{T}} > 25$ GeV and $p_{\mathrm{T}} > 27$ GeV for the 2015 and 2016–2018 data taking periods, respectively. These selections created three sub channels in the dilepton decay channel: ee (exactly 2 electrons with sufficient p_{T}), $\mu\mu$ (exactly 2 muons with sufficient p_{T}) and $e\mu$ (exactly 1 electron and 1 muon with sufficient p_{T}). Events are also required to have at least two of them with $p_{\mathrm{T}} > 25$ GeV, at least two of which have to be b-tagged by the MV2c10 tagger at 60 % efficiency working point. This selection is used in order to suppress non-$t\bar{t}$ backgrounds. A window of the lepton invariant mass, $m_{\ell\ell}$, at 80 GeV $< m_{\ell\ell} <$ 100 GeV is excluded in the ee and $\mu\mu$ channels to suppress the Z+jets background which resonates at the Z boson mass of around 91 GeV. Furthermore, a requirement of $E_{\mathrm{T}}^{\mathrm{miss}} > 60$ GeV is used in ee and $\mu\mu$ channels to account for the two neutrinos produced in the dilepton decay of $t\bar{t}$ and to suppress Z+jets contribution. The Z boson mass window and the $E_{\mathrm{T}}^{\mathrm{miss}}$ requirements are not imposed on the $e\mu$ channel because in the SM, the Z boson decays into leptons of the same flavour[1]. All three channels are also required to have $m_{\ell\ell} > 15$ GeV to reduce events where leptons originate from meson decays or photon conversions.

Considered backgrounds that could mimic the signal include: single top-quark production, W+jets processes (lepton+jets only), Z+jets, diboson processes (ZZ, WZ and WW), and associated production of $t\bar{t}$ with a Z, W or the Higgs bosons. The multijet background is estimated using a data-driven matrix method [15] in the lepton+jets channel and is estimated from simulation in the dilepton channel. Control histograms that compare observed data and the prediction from simulation show good agreement for various basic kinematic distributions.

[1] One electron and one muon can originate from the Z boson decay when the Z boson decays into a pair of tau leptons and they subsequently decay into one electron and one muon. However this is heavily suppressed by low branching fraction of both tau leptons decaying leptonically.

3 Event reconstruction

As top quarks decay before hadronisation, their four-momenta can only be reconstructed from their decay products: quarks and the (charged) lepton(s). Hence, the identification of jets corresponding to the partons from the $t\bar{t}$ decay is a crucial step of the direct top-quark decay width measurement as it allows to construct observables that are sensitive to the decay width. However, no prior information can be utilised to unambiguously identify the jet-to-parton assignment, thus some reconstruction algorithm has to be used. The $t\bar{t}$ reconstruction poses different problems in the lepton+jets and in the dilepton decay channels. In the lepton+jets channel, the difficulty of the reconstruction arises from the number of possible jet-to-parton assignments, referred to as a combinatorial background. On the other hand, in the dilepton channel, the combinatorial background is significantly reduced due to the smaller average number of jets in events compared to the lepton+jets case. However, presence of two prompt neutrinos means the system of equations that can be used to calculate the neutrino four-momenta using the W masses is under-constrained.

3.1 Lepton+jets reconstruction

Due to the large combinatorial background, the lepton+jets reconstruction technique chosen in the analysis makes use of a multivariate BDT technique. In a decision tree, ordered decision nodes are used to identify the event as a signal or a background event. Each node decides if the event is signal-like or background-like based on a single variable. Multiple decision nodes form a decision tree. Training is a process to identify the optimal order of the decision nodes as well as the optimal selection threshold in each node. During the training process, a selection is applied to the variable with the highest separation in the first node and then repeating the process for each subsample creating two new nodes during each step. This process is terminated when a certain node reaches maximum separation power, the minimum number of events is used or the maximum number of subsequent decisions (5) is made. Boosting of the decision trees means that signal events that end in the background category are assigned a larger weight than events correctly categorised and a new training with adjusted weights is performed. To combine the information from multiple trees a likelihood discriminant is built from all trees based on how often the signal event is correctly flagged as signal event in the decision trees. Different kinematic variables obtained from the reconstructed objects four-momenta as well as additional variables utilising the b-tagging information are provided to the BDT algorithm to identify the correct jet-to-parton assignment. One of the input variables is KLFitter $\ln\mathcal{L}$ which is the logarithm of the likelihood provided by the KLFitter reconstruction algorithm [16]. Permutations of jet-to-parton assignments are evaluated by the BDT and the per-

mutation with the highest BDT discriminant value is considered to be the correct permutation and is used further in the analysis. Electron+jets and muon+jets events are trained together in the training algorithms. From each background category, only the permutation with the highest KLFitter Event Probability is used further in the training process[1]. Taking only the permutation with the highest KLFitter Event Probability selects permutations with similar kinematics and b-tagging information as the signal permutation, thus making the separation between signal and background more difficult, in order to improve the overall performance of the training process. The BDT reconstruction efficiency is visualised in Figure 3.1 where the BDT score for the best considered permutation is shown.

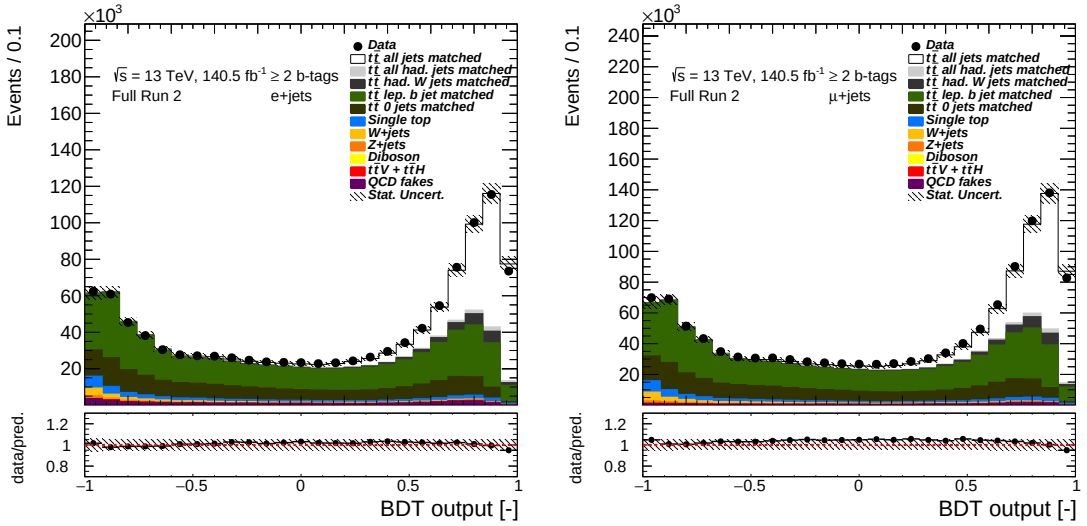

Figure 3.1: Data/Monte Carlo (MC) agreement of the BDT discriminant for electron+jets (left) and muon+jets (right) events. Signal $t\bar{t}$ events are split into reconstruction categories based on the reconstruction performance of the BDT. Only the permutation with the highest BDT score is shown. The hashed bands show the uncertainty originating from finite number of events in the MC modelling as well as normalisation uncertainty on each signal/background source. The first and last bin contain underflow and overflow events, respectively.

3.2 Dilepton reconstruction

The invariant mass of the charged lepton (electron or muon) and the corresponding b-jet from the same top quark decay, $m_{\ell b}$, is used as an observable sensitive to the top-

[1]The KLFitter Event Probability is not identical to the KLFitter likelihood value which is used as one of the input variables for the BDT. The KLFitter Event Probability takes into account b-tagging information while the KLFitter likelihood takes into account purely kinematic properties and no b-tagging information

quark decay width in the dilepton channel. Thus the problem of event reconstruction significantly simplifies since only the correct identification of the charged lepton with the corresponding b-jet is required. Two different approaches for the reconstruction in the dilepton channel have been tested. The first approach (referred to as minimum ΔR) uses the angular separation to match jets to their corresponding leptons. Events having two or more b-tagged jets are reconstructed by calculating ΔR between all possible combinations of leptons and b-tagged jets and consequently assigning the first lepton (ordered in p_{T}) to the closest b-tagged jet in ΔR and the second lepton to the closest non-assigned b-tagged jet. A b-jet is considered correctly matched if its ΔR distance from the corresponding truth b-quark from the $t\bar{t}$ decay is not greater than $\Delta R = 0.3$. The second approach (referred to as *minimum* $m_{\ell b}$) performs the pairing by searching for such a combination of the two charged leptons and two jets which minimises the difference in the combined invariant mass of the two ℓb systems. The $m_{\ell b}$ distribution has an upper limit originating from the mass of the top quark. As a consequence, incorrectly matched lepton-to-jet pairs are more likely to have larger invariant mass. Although the minimum $m_{\ell b}$ algorithm was found to be little more efficient than the ΔR pairing, as shown in Table 3.1, it is not used in the analysis since the usage of the same variable for both the reconstruction and the template fit might bias the top-quark decay width measurement and the reconstruction efficiency is similar between the two methods.

Reconstruction method [%]	b from t	b from $\bar{t}$	both b
Minimum ΔR	69	69	63
Minimum $m_{\ell b}$	69	69	66

Table 3.1: Efficiencies of charged lepton and corresponding b-jet pairing in percentages. The minimum ΔR and the minimum $m_{\ell b}$ reconstruction algorithms are compared in the $e\mu$ channel. The highlighted column (in grey) marks the pairing efficiency that is important for the top-quark decay width measurement. One event can fall into multiple categories. Statistical uncertainties on the efficiencies are below 1 % and are thus negligible. The high efficiency for reconstruction of both b-jets (last column) with respect to the individual b-jet reconstruction efficiencies reflects a high correlation of the reconstruction between the individual b-jets.

4 Analysis strategy

Distribution of variables sensitive to the top-quark decay width corresponding to different underlying Γ_t, width templates, are fitted to the observed data to extract the decay width. Due to the absence of the dedicated MC samples, the width templates are generated from the nominal $t\bar{t}$ sample, with $m_t = 172.5$ GeV and $\Gamma_t = 1.32$ GeV by reweighting utilising the parton truth information[1]. The reweighting uses theoretical Breit-Wigner distribution, BW(x), which describes the parton-level top-quark mass distribution

$$\mathrm{BW}(x) = \frac{2\sqrt{2}m_t\Gamma_t\sqrt{m_t^2(m_t^2+\Gamma_t^2)}}{\pi\sqrt{m_t^2+\sqrt{m_t^2(m_t^2+\Gamma_t^2)}}\cdot((x^2-m_t^2)^2+m_t^2\Gamma_t^2)}, \tag{4.1}$$

where m_t is set to 172.5 GeV. The masses x represent the truth top-quark masses from the MC truth record for top-quarks after final state radiation but before the decay of the particles. The values x vary on an event-by-event basis. To generate a distribution that corresponds to the given top-quark decay width Γ_t^{new}, a per-event-weight equal to the ratio of the BW functions is assigned where the nominator corresponds to the Breit-Wigner function with $\Gamma_t = \Gamma_t^{\mathrm{new}}$ and the top-quark mass equal to the truth top mass of the semileptonically decaying top quark for distributions created from semileptonically decaying top quarks in the case of lepton+jets events, and similarly for the dilepton events. The denominator represents the Breit-Wigner function with the top-quark decay width $\Gamma_t = 1.32$ GeV and the top-quark mass $m_t = 172.5$ GeV corresponding to the nominal MC $t\bar{t}$ sample. Using the reweighting procedure, distributions for any top-quark decay width value can be generated. In the 8 TeV analysis the width templates are generated in steps of 0.1 GeV in the range $0.1 < \Gamma_t < 5.0$ GeV with additional templates for $\Gamma_t = 0.01, 6, 7, 8$ GeV to account for very small and very large decay widths. The 13 TeV measurement uses templates corresponding to decay widths of $\Gamma_t = 0.2, 0.4, 0.7, 1.0, 1.4, 1.8, 2.2, 2.6, 3.0, 3.5, 4.0$ GeV in both considered $t\bar{t}$ decay channels. The differences between the steps in the templates arise from the difference in the fitting strategy.

The process of template creation has been validated using dedicated simulated samples with $\Gamma_t = 0.7$ and 3.0 GeV.

4.1 8 TeV fit strategy

Besides the changes in the detector and the LHC conditions, kinematics and cross-sections depend on the centre-of-mass energy. Due to the relatively larger contribution

[1] For the 8 TeV measurement, the decay width of the top quark was set to 1.33 GeV for the top-quark mass of 172.5 GeV.

of the W+jets background in the 8 TeV measurement compared to the 13TeV, measurement, the background has been split based on the flavour composition of the jets into events with the W boson and light jets (W+light), events with the W boson and c-jets (W+c) and events with at least two b or c-jets (W+bb/cc). The normalisation of each W+jets component is measured by in-situ techniques in the measurement of the $t\bar{t}$ charge asymmetry [17]. In the 8 TeV measurement, event selection in the lepton+jets channel similar to the selection outlined in Chapter 2 has been employed with one significant difference that at least one b-tagged jet has been required at 70 % b-tagging efficiency. Even though, events with exactly one b-tagged jet have larger non-$t\bar{t}$ background contamination compared to events with two b-tagged jets, considering the reduced number of $t\bar{t}$ events in the 8 TeV data taking requires to use even less pure events to reduce the statistical uncertainty of the measurement.

To maximise the shape information, the events passing the selection were split into 8 mutually orthogonal regions based on the lepton flavour, electron+jets and muon+jets channel; based on the number of b-tagged jets, exactly one b-tagged jet and more than one b-tagged jet; and finally based on the jet $|\eta|$, into regions where all four jets identified to be from the $t\bar{t}$ decay have $|\eta| < 1$ and the events where at least one jet has $|\eta| > 1$. The split into the flavour channels and number of b-tags is motivated by the different background compositions in the different regions as well as different sensitivity to the systematic uncertainties originating from the uncertainty on the flavour-tagging and charged lepton related uncertainties (efficiency of identification, triggering, energy and momentum scale and resolution).

A binned likelihood fit is set up to extract the Γ_t exploiting the templates fr the signal $t\bar{t}$ contribution. The distributions for the background processes are fixed in the fit. The normalisation of the $t\bar{t}$ is left free floating in the fit, while the normalisation of backgrounds is allowed to fluctuate within Gaussian constrains.

4.2 13 TeV fit strategy

The measurement with the 13 TeV dataset exploits a modified profile likelihood technique. The profile likelihood technique is a method how to include the effects of systematic uncertainties directly in the fit to the data that provides a coherent statistical interpretation. Each source of systematic uncertainty is described by a single nuisance parameter (NP) with the uncertainty that is measured in a dedicated *auxiliary* measurement. Likelihood with the NPs reads

$$\mathfrak{L}(n, \theta^{\mathbf{0}}|\mu, \theta) = \prod_{b \in \text{bins}} \text{Poisson}\left(n_b|\nu_b\right) \times \prod_{j \in \text{syst}+\gamma} f\left(a_j|\alpha_j\right), \tag{4.2}$$

where n_b describes the number of data events in a bin b. The term $f\left(a_j|\alpha_j\right)$ denotes the constrain term from the auxiliary measurement a_j that constrains NP α_j for the

source of systematic uncertainty j, including uncertainties that are fully decorrelated between the individual bins, γ.

The above mentioned likelihood provides a powerful tool for measurements of cross-sections, more precisely, signal strength, but it does not provide an optimal tool for fitting of shapes which is crucial for the template fit needed for the decay width measurement. The main problem arises from the fact that the standard profile likelihood implementation allows only 1 σ variations for the histogram, which is insufficient for the width measurement as more than 3 templates are used in the measurement. The approach chosen for the analysis transforms the problem of fitting of shapes into a well known problem of normalisation fitting. Symbolically, this can be expressed by the transformation

$$\mu S_b(\theta) \rightarrow S_b(\mu, \theta). \tag{4.3}$$

To achieve this transformation, an interpolation between the width templates is employed. The normalisation of width templates, T_i, is additionally weighted with w_i that depends on Γ_t representing template i and it can be expressed as

$$T(\Gamma_t) = \sum_{i=0}^{N} w_i(\Gamma_t) T_i. \tag{4.4}$$

The simplest expression for the weight w_i uses a piece-wise linear interpolation

$$w_i(\Gamma_t) = \begin{cases} 0 & \text{if} \quad \Gamma_t < \Gamma_{t,i-1}, \\ 1 - \frac{\Gamma_{t,i} - \Gamma_t}{\Gamma_{t,i} - \Gamma_{t,i-1}} & \text{if} \quad \Gamma_{t,i-1} < \Gamma_t < \Gamma_{t,i}, \\ 1 - \frac{\Gamma_t - \Gamma_{t,i}}{\Gamma_{t,i+1} - \Gamma_{t,i}} & \text{if} \quad \Gamma_{t,i} < \Gamma_t < \Gamma_{t,i+1}, \\ 0 & \text{if} \quad \Gamma_t > \Gamma_{t,i+1}. \end{cases}$$

Several procedures have been employed to validate the fitting procedure. The tests for the linearity of the response to the decay width rely on the fits of the width templatesto a combination of background templates and a $t\bar{t}$ signal template with a fixed Γ_t, the so called *Asimov fits*. The tests are carried out to check the mean value of the fitter Γ_t. The mean values obtained from the fit deviate up to 0.02 GeV with the input values for Γ_t, validating the chosen procedure.

5 Results

5.1 8 TeV result

Concatenated distributions of $m_{\ell b}$ and $\Delta R_{\min}(j_b, j_l)$ are split into 8 orthogonal regions and are simultaneously fitted to the data using a binned likelihood template fit. Figure 5.1 displays the likelihood curve of the fit of the 55 width templates considered in the fit. The quadratic fit to the likelihood points which follow the parabolic shapes are shown. The likelihood values, given as twice the negative logarithm of the likelihood, $-2\Delta\mathfrak{L}$, are shifted so that the minimum of the curve corresponds to $-2\Delta\mathfrak{L} = 0$. The statistical uncertainty, which includes the contributions from the finite number of the data events and normalisation of the backgrounds, is inferred from the likelihood curve as the width of the curve at $-2\Delta\mathfrak{L} = 1$ around the minimum.

The measured decay width reads

$$\Gamma_t = 1.76 \pm 0.33(\text{stat.})^{+0.79}_{-0.68}(\text{syst.})\ \text{GeV} = 1.76^{+0.86}_{-0.76}\ \text{GeV}, \tag{5.1}$$

assuming the top-quark mass $m_t = 172.5$ GeV. The result is in good agreement with the SM prediction of $\Gamma_t = 1.322$ GeV corresponding to NNLO corrections [12]. The measurement has been published in European Physics Journal C [18].

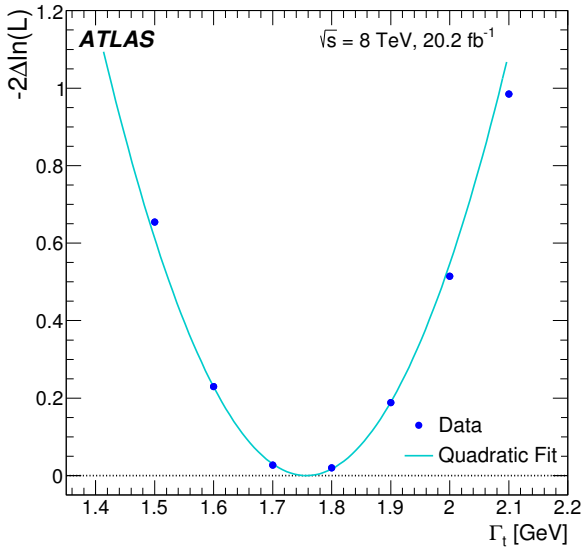

Figure 5.1: Likelihood curves obtained from the binned likelihood fit to the data. The quadratic fit to the likelihood points illustrated the parabolic behaviour of the fit.

5.2 13 TeV results

5.2.1 Lepton+jets results

A profile likelihood fit is employed to extract the top-quark decay width from the observed data collected by the ATLAS detector between years 2015–2018 for events that pass the lepton+jets selection described in Chapter 2. Templates corresponding to various input decay widths are constructed for the $m_{\ell b}$ observable from the combined distributions from the electron+jets and the muon+jets channel. Additionally, a control region comprised of the distribution of the reconstructed W boson mass in the combined electron+jets and muon+jets channel is used to control and constrain the dominant systematic uncertainties considered in the analysis. The measured top-quark decay width in the lepton+jets channel is

$$\Gamma_t = 1.30^{+0.50}_{-0.59}\ \text{GeV}, \tag{5.2}$$

assuming $m_t = 172.5$ GeV.

The likelihood scan of the parameter of interest, the decay width is shown in Figure 5.2.

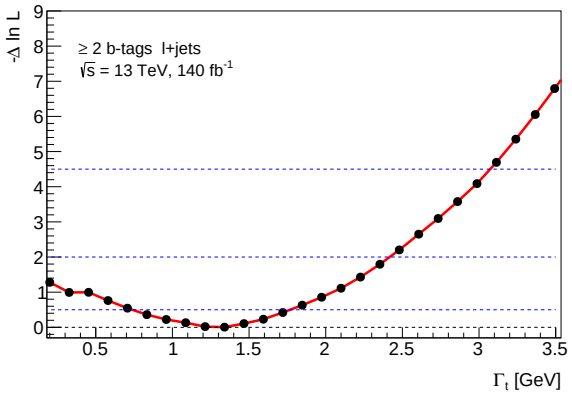

Figure 5.2: The likelihood scan for Γ_t in the lepton+jets.

5.2.2 Dilepton results

Data collected by the ATLAS detector between years 2015–2018 passing the dilepton selection summarised in Chapter 2 are fitted using the profile likelihood technique. The $m_{\ell b}$ distribution of $e\mu$ is used as an observable sensitive to the top-quark decay width, while the m_{bb} distribution for $\ell\ell$ events (events with the same flavour of the charged leptons) is used a control region in the fit. The top-quark decay width in the dilepton channel is found to be

$$\Gamma_t = 1.89^{+0.49}_{-0.47} \text{ GeV}, \tag{5.3}$$

assuming $m_t = 172.5$ GeV. The likelihood scan of the Γ_t is shown in Figure 5.3.

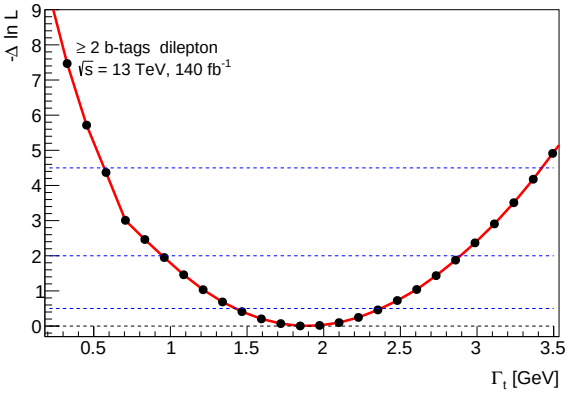

Figure 5.3: The likelihood scan for Γ_t in the dilepton channel.

5.2.3 Combination

Due to the orthogonal selection that is applied to the lepton+jets and the dilepton channels, the simulated MC and the observed data distributions are statistically independent. Systematic uncertainties are treated as fully correlated between the channels for all sources of uncertainties with the exception of the $t\bar{t}$ modelling uncertainties, that are uncorrelated between the regions. Motivation to decorrelate the $t\bar{t}$ modelling uncertainties stems from the fact that these uncertainties are significantly constrained thus by decorrelating them a more conservative approach is used. Normalisation of $t\bar{t}$ signal, which is a free floating parameter in both channels is also fully correlated in the combined fit. Finally, top-quark decay width values of templates have been chosen to be the same for both channels to simplify the combination. The combined fit yields

$$\Gamma_t = 1.46^{+0.30}_{-0.27} \text{ GeV}, \tag{5.4}$$

assuming $m_t = 172.5$ GeV.

Bibliography

[1] *Review of Particle Physics*, Phys. Rev. D **98** (2018) 030001.

[2] I. I. Y. Bigi, et al., *Production and Decay Properties of Ultraheavy Quarks*, Phys. Lett. B **181** (1986) 157–163.

[3] W. Bernreuther, M. Fücker, and Z.-G. Si, *Weak interaction corrections to hadronic top quark pair production: Contributions from quark-gluon and b anti-b induced reactions*, Phys. Rev. D **78** (2008) 017503.

[4] M. Cacciari, et al., *Top-pair production at hadron colliders with next-to-next-to-leading logarithmic soft-gluon resummation*, Phys. Lett. B **710** (2012) 612–622.

[5] P. Bernreuther, M. Czakon, and A. Mitov, *Percent Level Precision Physics at the Tevatron: First Genuine NNLO QCD Corrections to* $q\bar{q} \to t\bar{t} + X$, Phys. Rev. Lett. **109** (2012) 132001.

[6] M. Czakon and A. Mitov, *NNLO corrections to top-pair production at hadron colliders: the all-fermionic scattering channels*, JHEP **12** (2012) 054.

[7] M. Czakon and A. Mitov, *NNLO corrections to top pair production at hadron colliders: the quark-gluon reaction*, JHEP **01** (2013) 080.

[8] M. Czakon, P. Fiedler, and A. Mitov, *Total Top-Quark Pair-Production Cross Section at Hadron Colliders Through* $O(\alpha_S^4)$, Phys. Rev. Lett. **110** (2013) 252004.

[9] M. Czakon and A. Mitov, *Top++: A Program for the Calculation of the Top-Pair Cross-Section at Hadron Colliders*, Comput. Phys. Commun. **185** (2014) 2930.

[10] A. D. Martin, et al., *Parton distributions for the LHC*, Eur. Phys. J. C **63** (2009) 189–285.

[11] M. Jezabek and J. H. Kuhn, *QCD Corrections to Semileptonic Decays of Heavy Quarks*, Nucl. Phys. B **314** (1989) 1–6.

[12] J. Gao, C. S. Li, and H. X. Zhu, *Top Quark Decay at Next-to-Next-to Leading Order in QCD*, Phys. Rev. Lett. **110** (2013) 042001.

[13] ATLAS Collaboration, *The ATLAS Experiment at the CERN Large Hadron Collider*, JINST **3** (2008) S08003.

[14] ATLAS Collaboration, *Measurements of b-jet tagging efficiency with the ATLAS detector using $t\bar{t}$ events at $\sqrt{s} = 13$ TeV*, JHEP **08** (2018) 089.

[15] D0 Collaboration, *Measurement of the $t\bar{t}$ production cross section in $p\bar{p}$ collisions at $\sqrt{s} = 1.96$ TeV using kinematic characteristics of lepton + jets events*, Phys. Rev. D **76** (2007) 092007.

[16] J. Erdmann, et al., *A likelihood-based reconstruction algorithm for top-quark pairs and the KLFitter framework*, Nucl. Instrum. Meth. A **748** (2014) 18–25.

[17] ATLAS Collaboration, *Measurement of the charge asymmetry in top-quark pair production in the lepton-plus-jets final state in pp collision data at $\sqrt{s} = 8$ TeV with the ATLAS detector*, Eur. Phys. J. C **76** (2016) 87, [Erratum: Eur. Phys. J.C77,564(2017)].

[18] ATLAS Collaboration, *Direct top-quark decay width measurement in the $t\bar{t}$ lepton+jets channel at $\sqrt{s}$ =8 TeV with the ATLAS experiment*, Eur. Phys. J. C **78** (2018) 129.

Author's Publications

1. ATLAS Collaboration, *Direct top-quark decay width measurement in the $t\bar{t}$ lepton+jets channel at $\sqrt{s} = 8$ TeV with the ATLAS experiment*, Eur. Phys. J. C 78 (2018) 129

2. Tomáš Dado (on behalf of the ATLAS Collaboration), *Top-quark properties and mass measurements with the ATLAS detector*, EPJ Web of Conferences, Volume 182 (2018)

3. Tomáš Dado (on behalf of the ATLAS Collaboration), *Top quark properties and mass measurements with ATLAS*, Nuclear and Particle Physics Proceedings, Volumes 300–302 (2018)

4. ATLAS Collaboration, *Measurement of the top quark mass in the $t\bar{t} \to$dilepton channel from $\sqrt{s} = 8$ TeV ATLAS data*, Phys. Lett. B 761 (2016) 350–371

5. ATLAS Collaboration, *Measurement of the $t\bar{t}Z$ and $t\bar{t}W$ production cross sections in multilepton final states using 3.2 fb^{-1} of pp collisions at $\sqrt{s} = 13$ TeV with the ATLAS detector*, Eur. Phys. J. C 77 (2017) no.1, 40

6. ATLAS Collaboration, *Measurements of top quark spin observables in $t\bar{t}$ events using dilepton final states in $\sqrt{s} = 8$ TeV pp collisions with the ATLAS detector* , JHEP 1703 (2017) 113

7. ATLAS Collaboration, *Search for top quark decays $t \to qH$, with $H \to \gamma\gamma$, in $\sqrt{s} =$ 13 TeV pp collisions using the ATLAS detector*, JHEP 1710 (2017) 129

8. ATLAS Collaboration, *Measurements of top-quark pair differential cross-sections in the lepton+jets channel in pp collisions at $\sqrt{s} = 13$ TeV using the ATLAS detector*, JHEP 1711 (2017) 191

9. ATLAS Collaboration, *Evidence for the $H \to b\bar{b}$ decay with the ATLAS detector*, JHEP 1712 (2017) 024

10. ATLAS Collaboration, *Observation of Higgs boson production in association with a top quark pair at the LHC with the ATLAS detector*, Phys. Lett. B 784 (2018) 173–191

11. ATLAS Collaboration, *Probing the quantum interference between singly and doubly resonant top-quark production in pp collisions at $\sqrt{s} = 13$ TeV with the ATLAS detector*, Phys. Rev. Lett. 121 (2018) no.15, 152002

12. ATLAS Collaboration, *Observation of $H \to b\bar{b}$ decays and VH production with the ATLAS detector*, Phys. Lett. B 786 (2018) 59–86

13. ATLAS Collaboration, *Measurement of colour flow using jet-pull observables in $t\bar{t}$ events with the ATLAS experiment at $\sqrt{s} = 13$ TeV*, Eur. Phys. J. C 78 (2018) no.10, 847

14. ATLAS Collaboration, *Measurement of the W boson polarisation in $t\bar{t}$ events from pp collisions at $\sqrt{s} = 8$ TeV in the lepton+jets channel with ATLAS* , Eur. Phys. J. C 78 (2018) no.10, 847